Radboud Repository

Radboud University Nijmegen

PDF hosted at the Radboud Repository of the Radboud University Nijmegen

The following full text is a publisher's version.

For additional information about this publication click this link.
http://hdl.handle.net/2066/168325

Please be advised that this information was generated on 2021-11-07 and may be subject to change.

Biallelic Mutations in *CRB1* Underlie Autosomal Recessive Familial Foveal Retinoschisis

Ajoy Vincent,[1–3] Judith Ng,[1] Christina Gerth-Kahlert,[4] Erika Tavares,[1] Jason T. Maynes,[5] Thomas Wright,[2] Amit Tiwari,[6] Anupreet Tumber,[2] Shuning Li,[1] James V. M. Hanson,[4] Angela Bahr,[6] Heather MacDonald,[2,7,8] Luzy Bähr,[6] Carol Westall,[2,3] Wolfgang Berger,[6,9,10] Frans P. M. Cremers,[11] Anneke I. den Hollander,[11,12] and Elise Héon[1–3]

[1]Program of Genetics and Genome Biology, The Hospital for Sick Children, Toronto, Canada
[2]Department of Ophthalmology and Vision Sciences, The Hospital for Sick Children, University of Toronto, Toronto, Canada
[3]Department of Ophthalmology and Vision Sciences, University of Toronto, Toronto, Canada
[4]Department of Ophthalmology, University Hospital Zurich, Zurich, Switzerland
[5]Department of Anesthesia and Pain Medicine, and Program in Molecular Structure and Function, The Hospital for Sick Children, Toronto, Canada
[6]Institute of Medical Molecular Genetics, University of Zürich, Wagistrasse 12, Schlieren, Switzerland
[7]Department of Molecular Genetics, University of Toronto, Toronto, Ontario, Canada
[8]Division of Clinical and Metabolic Genetics, The Hospital for Sick Children, Toronto, Ontario, Canada
[9]Zurich Center for Integrative Human Physiology (ZIHP), University of Zürich, Zürich, Switzerland
[10]Neuroscience Center Zurich (ZNZ), University and ETH Zürich, Zürich, Switzerland
[11]Department of Human Genetics, Radboud University Medical Centre, Nijmegen, The Netherlands
[12]Department of Ophthalmology, Radboud University Medical Centre, Nijmegen, The Netherlands

Correspondence: Elise Héon, Department of Ophthalmology and Vision Sciences, The Hospital for Sick Children, 555 University Avenue, Toronto, Ontario M5G 1X8, Canada;
elise.heon@sickkids.ca.

Submitted: September 27, 2015
Accepted: March 19, 2016

Citation: Vincent A, Ng J, Gerth-Kahlert C, et al. Biallelic mutations in *CRB1* underlie autosomal recessive familial foveal retinoschisis. *Invest Ophthalmol Vis Sci*. 2016;57:2637–2646. DOI:10.1167/iovs.15-18281

Purpose. To identify the genetic cause of autosomal recessive familial foveal retinoschisis (FFR).

Methods. A female sibship with FFR was identified (Family-A; 17 and 16 years, respectively); panel based genetic sequencing (132 genes) and comparative genome hybridization (142 genes) were performed. Whole-exome sequencing (WES) was performed on both siblings using the Illumina-HiSeq-2500 platform. A sporadic male (Family-B; 35 years) with FFR underwent WES using Illumina NextSeq500. All three affected subjects underwent detailed ophthalmologic evaluation including fundus photography, autofluorescence imaging, spectral-domain optical coherence tomography (SD-OCT), and full-field electroretinogram (ERG).

Results. Panel-based genetic testing identified two presumed disease causing variants in *CRB1* (p.Gly123Cys and p.Cys948Tyr) in Family-A sibship; no deletion or duplication was detected. WES analysis in the sibship identified nine genes with two or more shared nonsynonymous rare coding sequence variants; *CRB1* remained a strong candidate gene, and *CRB1* variants segregated with the disease. WES in Family-B identified two presumed disease causing variants in *CRB1* (p.Ile167_Gly169del and p.Arg764Cys) that segregated with the disease phenotype. Distance visual acuity was 20/40 or better in all three affected except for the left eye of the older subject (Family-B), which showed macular atrophy. Fundus evaluation showed spoke-wheel appearance at the macula in five eyes. The SD-OCT showed macular schitic changes in inner and outer nuclear layers in all cases. The ERG responses were normal in all subjects.

Conclusions. This is the first report to implicate *CRB1* as the underlying cause of FFR. This phenotype forms the mildest end of the spectrum of *CRB1*-related diseases.

Keywords: retinoschisis, macular degeneration, macular edema, familial foveal retinoschisis, human CRB1 protein, optical coherence tomography, electroretinogram (ERG), electroretinography

Familial foveal retinoschisis (FFR) is an extremely rare autosomal recessive disorder first described by Lewis et al., in 1977.[1] Affected cases present within the first two decades of life with reduced distance visual acuity, usually in the range of 20/30 to 20/60. The retina shows the characteristic fovea centered cart-wheel lesion restricted to the macula; the peripheral retina is normal.[1–3] The cart-wheel lesions reflect schitic or cystoid changes, clearly evident on optical coherence tomography (OCT). Mild protan or tritan color vision anomalies may be observed. Full-field ERG is usually normal in keeping with the maculopathy; however, the dim light scotopic ERG can be subnormal.[1] In 2003, Kabanarou et al.[2] introduced the term isolated foveal retinoschisis to accommodate both sporadic and familial cases

This work is licensed under a Creative Commons Attribution-NonCommercial-NoDerivatives 4.0 International License.

Downloaded from iovs.arvojournals.org on 07/09/2021

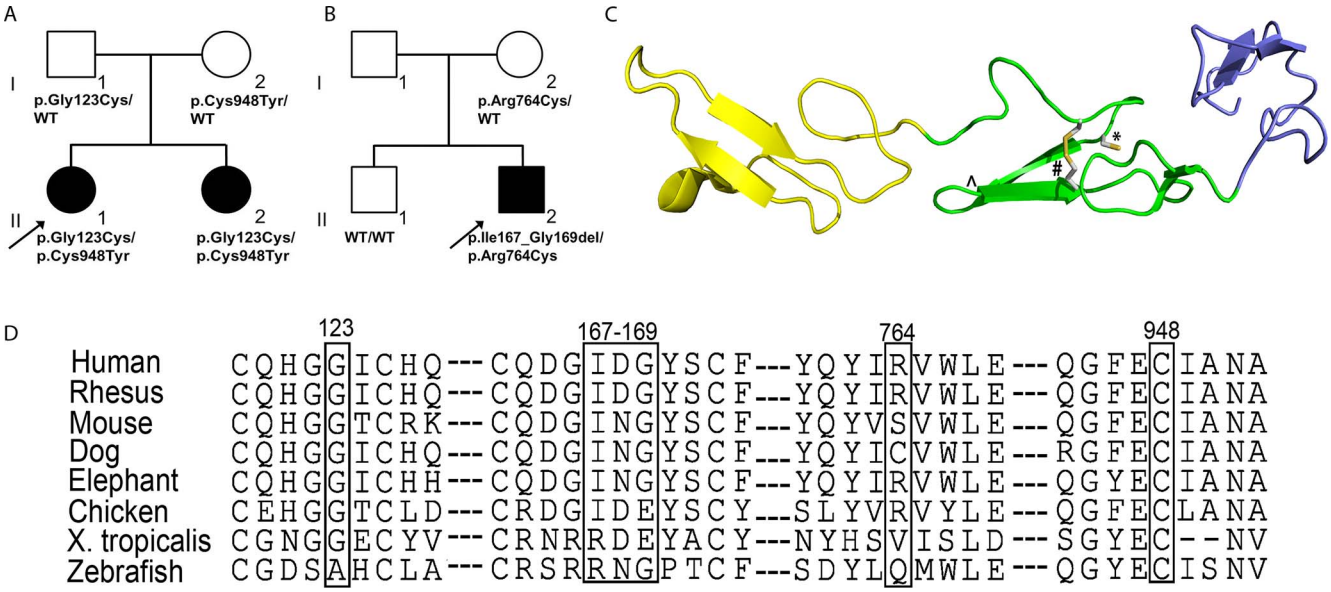

FIGURE 1. Pedigree, segregation analysis, protein structure, and conservation map. (**A**) Pedigree and segregation analysis of Family-A. (**B**) Pedigree and segregation analysis of family-B. (**C**) Epidermal growth factor–like domains form tandem repeats that create solenoid-like oligomeric structures. Using the x-ray crystal structure of Notch ligand delta-like 1 (PDB ID 4XBM),[52] the identified CRB1 mutations were mapped onto a typical EGF-like structure. Each EGF-like repeat is colored separately (*yellow* to *green* to *blue*). The Gly123Cys mutation lies in a turn region (*), disrupting EGF-like domain formation. The Cys948Tyr mutation disrupts a disulfide bridge, which are important for internal structural rigidity of the domain (disulfide shown by #). The caret (^) is the position of the residue 168, showing how a deletion would affect the beta-turn of the EGF-like domain. (**D**) Amino acid conservation map across species: The residues p.Gly123 and p.Cys948 (Family-A) are preserved lower down to xenopus and zebrafish, respectively. The residues p.Ile167 and p.Gly169 are conserved until chicken and elephant respectively; the residues p.Asp168 and p.R764 are conserved in Rhesus.

of the disorder. There is high female preponderance as all nine cases reported in literature are females; the reason for this is unknown[1–3] (Lorenz B, et al. *IOVS* 2000;41:ARVO Abstract S883).

In humans, *CRB1* is expressed in the retina and brain, and codes for the human orthologue of *Drosophila melanogaster* transmembrane protein Crumbs.[4] Alternate splicing leads to two isoforms, 1376 amino acids (AF_154671) and 1406 amino acids (NP_957705) in length.[4,5] Both isoforms have extracellular components; but the larger transcript also has transmembrane and cytoplasmic domains.[5] The cytoplasmic domain of the larger transcript is functionally conserved to Drosophila Crumbs, and is capable of partially rescuing Drosophila *Crumbs* mutants.[5] The Crumbs protein is a major determinant of epithelial polarity.[6]

Mapped to chromosome 1q31.3, *CRB1* mutations have been associated with a wide-range of retinal phenotypes that include Leber congenital amaurosis (LCA), early onset retinal dystrophy (EORD), retinitis pigmentosa (RP), and maculopathy.[4,7–10] *CRB1* has also been associated with a complex eye phenotype, nanophthalmos-RP-optic disc drusen, in a Turkish family.[11] The current study identifies the novel association of *CRB1* as the underlying cause of autosomal recessive FFR.

METHODS

The study protocol was approved by the Ethics Review Board of all participating hospitals, and followed the tenets of the Declaration of Helsinki. A female sibship of FFR (Fig. 1A; Family-A) was identified at The Hospital for Sick Children (HSC), Toronto, Canada. A sporadic male with isolated foveal retinoschisis (Fig. 1B; Family-B) was identified at the University Hospital, Zurich, Switzerland.

Clinical Evaluation

Four members in Family-A (proband [II-1], affected sibling [I-2], and unaffected parents) and proband from Family-B (II-2) underwent detailed eye examination including best corrected visual acuity (BCVA), fundus photography, fundus autofluorescence testing (FAF: Visucam$^{NM/FA}$; Carl Zeiss Meditec, Jena, Germany; or Spectralis, Heidelberg Engineering, Heidelberg, Baden-Württemberg, Germany) and spectral-domain OCT (SD-OCT; Cirrus; Carl Zeiss Meditec or Spectralis, Heidelberg Engineering).

Full-field ERG testing incorporating International Standards[12,13] and intravenous fluorescein angiography were performed on all three affected individuals. Goldmann Visual Fields (GVF) testing using both I4e and III4e isopters were performed in affected individuals in Family-A.

Segmentation analysis was performed on the SD-OCT from the left eye in all three affected individuals. In Family-A, a 6×6 mm region of retina centered on the fovea was scanned using the 512×128 macular cube protocol using Cirrus HD-OCT 5000. Control data was collected from one eye of 40 patients with normal visual development (median age: 23.5 years, range, 12–35 years), recruited as part of a separate study. Ten retinal layers were identified in each macular cube OCT using Iowa Reference Algorithms (Retinal Image Analysis Lab, Iowa Institute for Biomedical Imaging, Iowa City, IA, USA).[14–16] Custom software averaged thickness measurements over retinal regions corresponding to the three rings suggested by the Early Treatment Diabetic Retinopathy Study (ETDRS)[17]; the ETDRS ring design consists of a central foveal region with a 1-mm diameter, an inner ring with and inner and outer diameter of 1 and 3 mm, respectively, and an outer ring with inner and outer diameters of 3 and 6 mm, respectively. The OCT in family B was performed using Spectralis; a 30° (~8.3×8.3 mm) square centered on the fovea was scanned using the $1536 \times$

Investigative Ophthalmology & Visual Science

Downloaded from iovs.arvojournals.org on 07/09/2021

496 line protocol. The ETDRS regions were segmented and averaged using the built-in software on the system. The total retinal thickness and thickness of ganglion cell-inner plexiform complex (GCL-IPL; as it contained the least amount of schitic changes) were measured.

Genetic Testing

Family-A. Multistep clinical genetic testing was performed. In total, 132 genes known to cause retinal dystrophy were screened using PCR amplification and next-generation or Sanger sequencing (Supplementary Table S1). A comparative genomic hybridization technique was used to test for deletion or duplication in 142 genes associated with non-syndromic/syndromic inherited eye dystrophies (Supplementary Table S1). Whole exome capture and sequencing (WES) was performed in the two affected siblings at The Center for Applied Genomics (TCAG), Toronto, Canada and analyzed using standard pipeline (Supplementary Methods).[18] Overall mean target exon coverage was 101× and 110× in II-1 and II-2, respectively; 95% of targets in both siblings had a greater than 20× base coverage. The potential effect of rare (allele frequency ≤ 0.01) coding-sequence single nucleotide variants (SNVs) were predicted using six predictive tools that included Polyphen-2,[19] SIFT,[20] mutation assessor (Ma),[21] combined annotation-dependent depletion (CADD) Phred,[22] and conservation values amongst PhyloP placental mammals and PhyloP 100-vertebrates. A cut off score was set for each tool (Polyphen-2 ≥ 0.95; SIFT ≤ 0.05, Ma ≥ 2.0, CADD Phred ≥ 15, Average PhyloP nucleotide conservation inferred from placental mammal: value ≥ 1.0 and Average PhyloP nucleotide conservation inferred from 100 vertebrates: value ≥ 1.0). Any SNV that met the cut off for a specific predictive tool was given a score of 1; a maximum cumulative score of 6 was possible for any SNV. If a SNV did not meet the cut off for a specific tool, then a score of 0 was given.

Family-B. Genomic DNA was isolated from patients' blood sample and WES was performed using standard protocols (Supplementary methods). A filtering approach was established to exclude known single nucleotide polymorphisms or benign sequence variations. Mutations that have been previously described to be disease causing in the Human Gene Mutation Database and literature were given the highest priority followed by protein truncation mutations (nonsense and frameshift variants). Sequence variants considered relevant for the disease, were confirmed by conventional Sanger sequencing.

Results

Clinical Phenotype: Family-A

Proband (II-1). A 17-year-old female born to nonconsanguineous Caucasian parents (Fig. 1A) presented with a 4-year history of diminution in distance vision. There is no history suggestive of photophobia or nyctalopia. The BCVA was 20/30 and 20/40 in the right and left eyes, respectively. Color vision was normal in both red-green and blue-yellow axes. The contrast sensitivity was 1.35 log units in each eye. Fundus evaluation showed spoke-wheel appearance at the fovea in both eyes (Fig. 2A); the remainder of the retina was normal. On FAF, the spoke-wheel appeared hypointense, the AF level in the posterior pole was otherwise normal (Fig. 2B). The GVF was noted to be normal in either eye at 140° × 110° (III4e target; horizontal × vertical) and 125° × 100° (I4e target). The ERG recordings showed normal rod and cone responses (Fig. 3A) as seen in controls (Fig. 3C). The SD-OCT showed marked schitic changes at the macula in the inner and outer nuclear layers (Fig. 2C). Within the regions of schisis, localized areas of disruption of photoreceptor inner segments (IS) and outer segments (OS), and the external limiting membrane (ELM) were also noted (* in Fig. 2C). The central subfield thickness (1 mm) was measured to be 423 and 475 μm in the right and left eyes, respectively.

At the most recent follow-up visit at 22 years, all visual parameters including visual fields were unchanged. Fluorescein angiogram showed no leakage in the left eye; minimal leakage was noted in the right eye. The schitic changes at the macula improved on Dorzolamide 2% eye drops twice daily (Fig. 2D); the central subfield thickness reduced to 308 and 288 μm in the right and left eyes, respectively. The total retinal thickness and GCL-IPL thickness was within normal limits in the inner and outer rings, on two occasions (at 17 and 22 years; Figs. 4A, 4B).

Sibling (Case II-2). The 16-year-old sibling presented with a four year history of difficulty seeing at distance in the school; her symptoms have been stable over time. There was no history of photophobia or nyctalopia, but complained of taking longer to adapt to dimly lit environments.

On evaluation, the BCVA was 20/30 and 20/40 in the right and left eyes, respectively. Color vision was normal. The contrast sensitivity was 1.35 and 1.20 log units in the right and left eyes, respectively. Fundus evaluation showed dull macular reflex with cystoid changes in both eyes (Fig. 2E); the remainder of the retina was normal. The right eye FAF showed streaks of radial hyper-AF originating from the center; a few specks of absent AF were noted superonasal to the fovea. The FAF of the left eye showed a spoke-wheel pattern of hypointense AF (Fig. 2F). The GVF was noted to be normal in either eye at 135° × 105° and 120° × 90° for III4e and I4e stimulus targets, respectively. The ERG results showed normal dim-light scotopic response (DA 0.01) and normal cone responses; the combined maximal responses (DA2.29 and DA 7.6) showed low-normal a-wave amplitudes (Fig. 3B). The SD-OCT showed marked macular schitic changes in the inner and outer nuclear layers (Fig. 2G); these regions also showed localized areas of disruption in photoreceptor IS and OS, and the ELM (* in Fig. 2G). The central subfield thickness was 429 and 478 μm in the right and left eyes, respectively.

At the most recent follow-up visit at 21 years, BCVA was noted to be 20/25 and 20/30 in the right and left eyes, respectively (one line improvement on ETDRS chart). Fluorescein angiography showed no evidence of leakage in either eye. The SD-OCT demonstrated reduction in schitic changes on topical Dorzolamide 2% treatment (Fig. 2H); central subfield thickness was 291 and 314 μm in the right and left eyes, respectively. The central retinal thickness and GCL-IPL complex was thicker in most tested regions on both visits (16 and 21 years; Figs. 4A, 4B).

Cases I-1 and I-2. Both parents (53-years old) were asymptomatic and had completely normal eye examination including FAF. The SD-OCT showed normal central retinal thickness, layering, and morphology.

Clinical Phenotype: Family B

Case II-2. The 35-year-old male presented with bilateral reduced visual acuity and contrast vision for several years. Previous record suggested a diagnosis of bilateral maculopathy made at 7 years of age. There is no history suggestive of photophobia or nyctalopia. At 30 years of age, his BCVA was 20/80 in either eye. At the most recent follow-up (35 years), his BCVA was 20/40 and 20/200 in the right and left eyes, respectively. The fundus showed dull foveal reflex with cystoid changes in the right eye and dull macular reflex with minimal retinal pigment epithelium (RPE) changes in the left eye. The

Investigative Ophthalmology & Visual Science

Downloaded from iovs.arvojournals.org on 07/09/2021

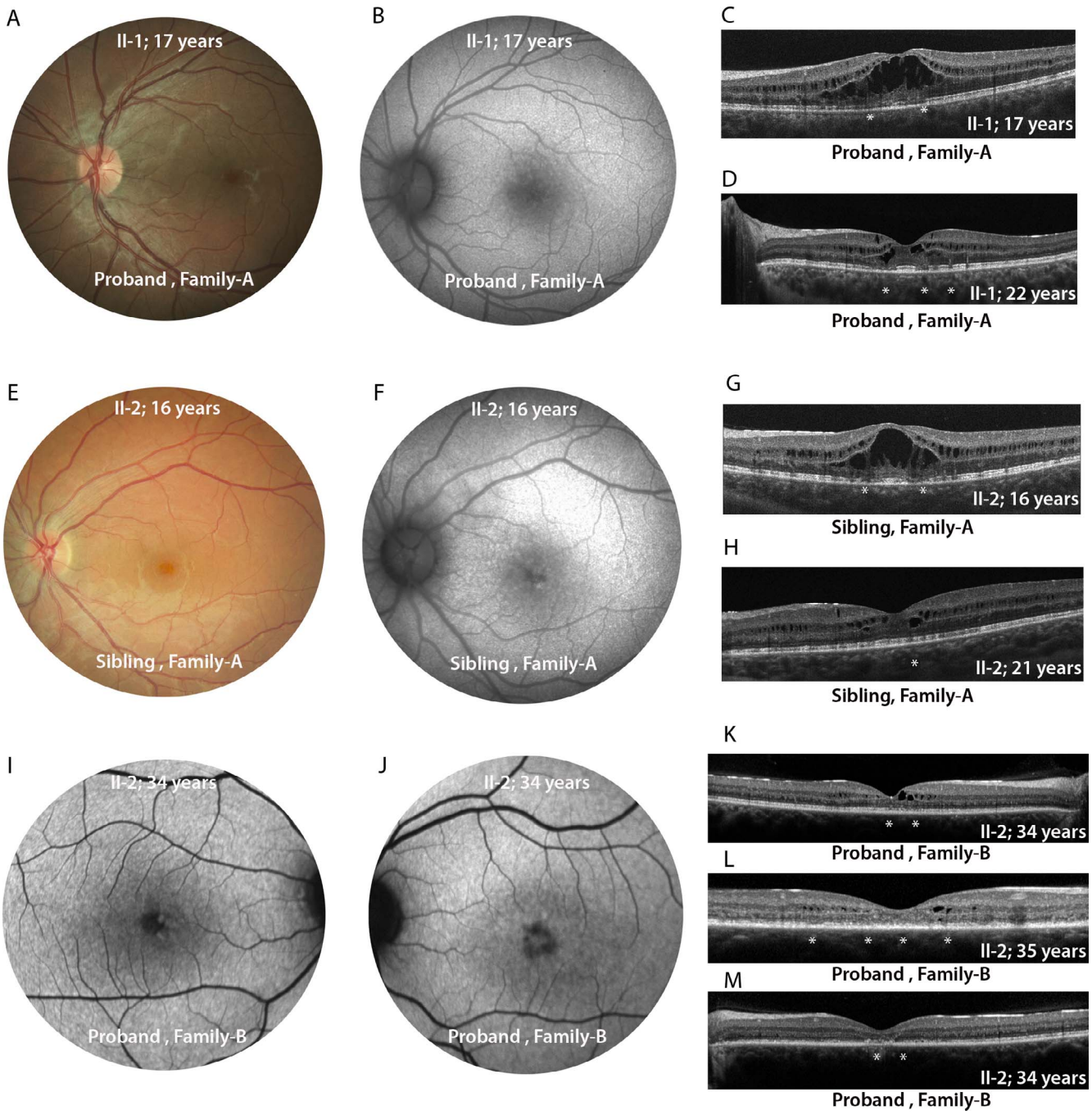

Figure 2. Detailed phenotypic characteristics of Family-A (Cases II-1 [**A**–**D**] and II-2 [**E**–**H**]) and Family-B (II-2; [**I**–**M**]). (**A**) Fundus photograph (II-1; Family-A) at 17 years showing dull foveal reflex with spoke wheel appearance at the fovea. (**B**) Fundus autofluorescence (II-1) showing the *spoke-wheel pattern* to be hypo-AF. (**C**, **D**) Spectral-domain OCT at 17 and 22 years, respectively. The SD-OCT initially showed marked macular schitic changes in the inner and outer nuclear layers (**C**). Schitic changes improved on topical dorzolamide (**D**). The SD-OCT also showed localized areas of disruption in photoreceptor IS and OS, and ELM (* in **C**, **D**). (**E**) Fundus photograph (II-2) at 16 years showing *spoke-wheel* appearance at the fovea. (**F**) Fundus autofluorescence (II-2) showing the *spoke-wheel pattern* to be hypo-AF. (**G**, **H**) Spectral-domain OCT (II-2) at 16 years and 21 years, respectively. The SD-OCT initially showed marked macular schitic changes in the inner and outer nuclear layers (**G**); schitic changes improved on topical dorzolamide (**H**). The SD-OCT also showed localized areas of disruption in photoreceptor IS and OS, and the ELM (* in **G**, **H**). (**I**, **J**) Fundus autofluorescence from right and left eyes respectively from II-2 (Family-B). The partial (**I**) and complete (**J**) *spoke-wheel* demonstrate hyperintense AF. (**K**–**M**) Spectral-domain OCT images from the *right* (**K**, **L**) and *left* (**M**) respectively. The schitic changes are noted only in the right eye (**K**, **L**). The left eye shows macular atrophy (**M**).

FAF showed a partial (right) or complete (left) spoke-wheel pattern of hyperintense AF; foveolar hyper-AF was noted in the left eye (Figs. 2I, 2J). Fluorescein angiography revealed no abnormalities in the right eye; presence of macular staining with no leakage was noted in the left eye. The ERG showed normal rod and cone responses. On SD-OCT, the right eye showed schitic changes, more so in the inner nuclear layer (Figs. 2K, 2L). In the left eye, macular atrophy was noted (Fig. 2M); both eyes showed disruptions in the photoreceptor IS and OS, and the ELM (* in Figs. 2K, 2L, 2M). The central retinal thickness was

Investigative Ophthalmology & Visual Science

Downloaded from iovs.arvojournals.org on 07/09/2021

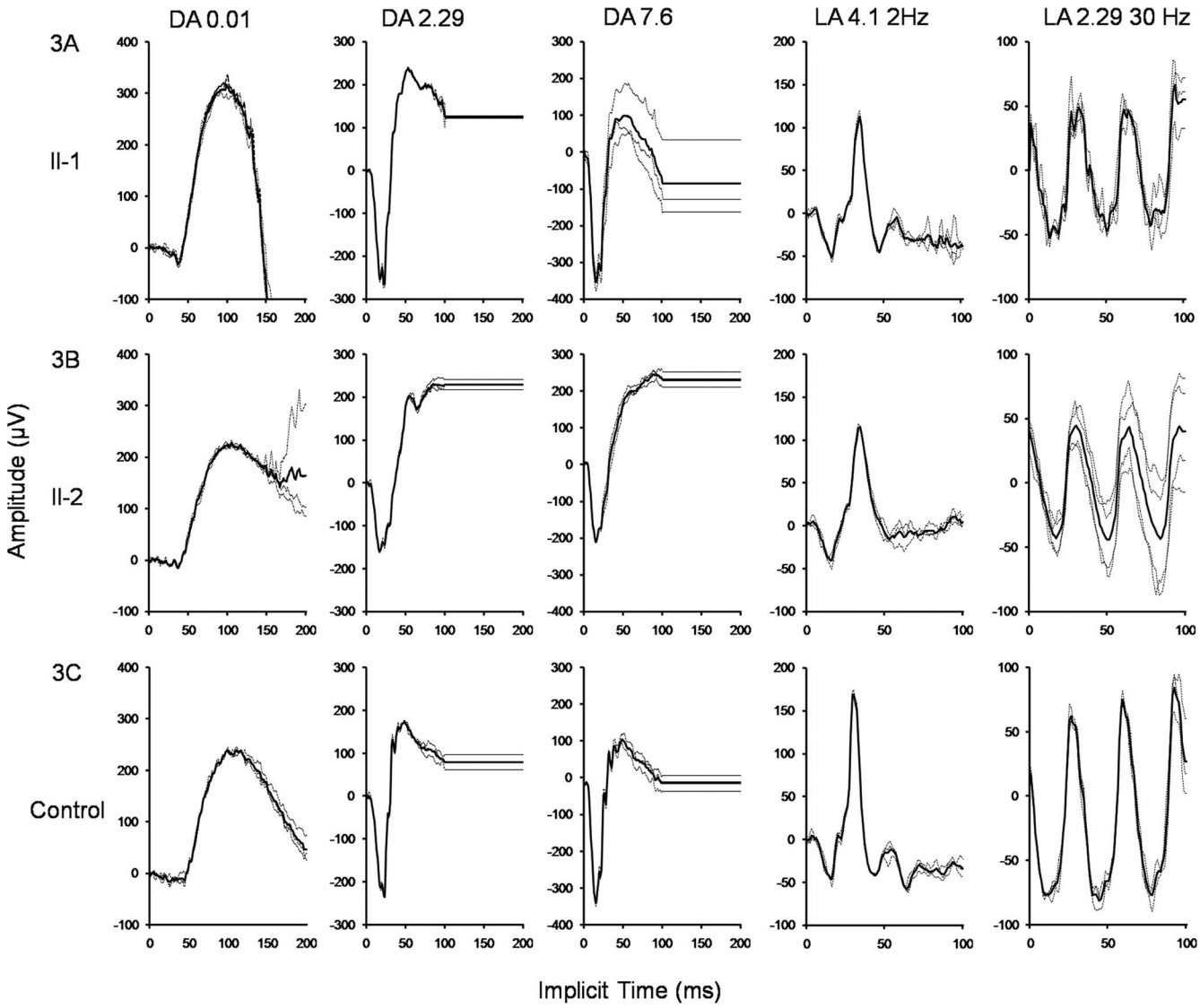

Figure 3. Electroretinogram results from the affected cases in Family-A. Adaptive status of the eye is labeled in dark adapted, DA; light adapted, LA. The stimulus intensities are represented in numerical form following the adaptive state; unit being candela-second per square meter. *Bold traces* are averaged responses; *broken line* represents response to individual flashes. (**A**) Recordings from the right eye of Case II-1. All rod responses (DA 0.01, 2.29, and 7.6) are normal. The single-flash photopic response (LA 4.1 2 Hz) and 30-Hz flicker response (LA 2.29 30 Hz) are normal. (**B**) Recordings from the left eye of Case II-2. Dim light scotopic response (DA 0.01) is normal; combined maximal responses (DA 2.29 and 7.6) show low-normal a-wave amplitude; b-wave amplitudes are normal. The single flash photopic response (LA 4.1 2 Hz) and 30-Hz flicker response (LA 2.29 30 Hz) are normal. (**C**) ERG trace from a control subject is shown for comparison.

reduced in most ETDRS rings consistent with macular atrophy (left eye); GCL-IPL thickness was either normal (1- to 3-mm ring) or increased (3- to 6-mm ring; Figs. 4A, 4B).

Genetic Results: Family-A

Among the 132 genes tested by sequencing, two likely disease causing variants were observed in *CRB1* (NM_201253) in both siblings. The changes are denoted as c.367G > T/p.Gly123Cys (novel rare variant) and c.2483G > A/p.Cys948Tyr (previously published).[6,23–26] No deletion or duplication was detected in *RS1* or any of the 141 eye disease associated genes tested.

Because FFR was different from other known *CRB1*-associated phenotypes, WES was performed.

The filtering steps used in the WES analysis of II-1 and II-2 are summarized in Table 1. In total, 540 nonsynonymous coding variants were classified as rare variants (see Methods). One hundred seventy-five of these rare coding variants were shared by the two individuals; among these, only nine genes had at least two shared variants amongst both siblings. None of the rare coding sequence variants shared amongst the sibship was in a homozygous state.

All shared SNVs in the nine genes were assessed (19 in total; *PCDHGB7* had 3 variants) and scored using the six predictive tools (see methods section) and cumulative score was calculated (Table 2). A minimum cut-off of 2/6 was set to prioritize pathogenicity of individual SNV. All genes that had two SNVs meeting the cut-off score were prioritized: *CRB1* and *SKOR1* (Table 2).

Both *CRB1* variants (c.367G > T/p.Gly123Cys and c.2483G > A/p.Cys948Tyr) had the maximum predictive score of six. Amongst the nine genes, only *CRB1* was previously associated with a human disease phenotype following a Mendelian pattern of inheritance (Table 1). Taken together, *CRB1* was considered

Investigative Ophthalmology & Visual Science

Downloaded from iovs.arvojournals.org on 07/09/2021

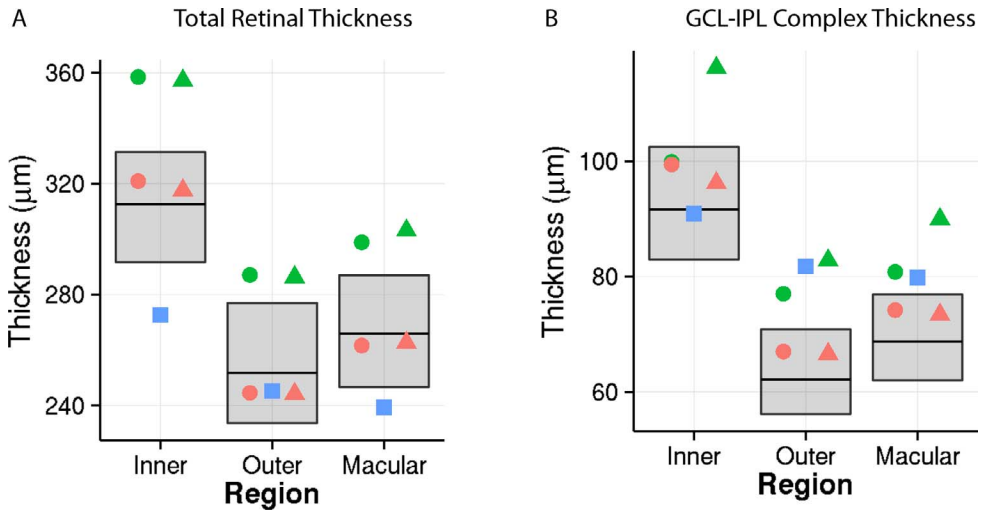

Figure 4. Segmentation analysis derived from macular cube scans of SD-OCT. Only left eye data was analyzed. The central 1-mm ring is not shown as it had significant schitic changes that impaired analysis. *Pink circle* and *triangle* represent first and last visits, respectively, in the proband of Family-A (II-1). *Green circle* and *triangle* represent first and last visits, respectively, in the affected sibling of the proband in Family-A (II-2). *Blue triangle* represents single test visit of the proband in Family-B. Inner corresponds to 1- to 3-mm ring, outer corresponds to 3- to 6-mm ring and macular corresponds to all three rings. (**A**) Represents total retinal thickness with the exclusion of retinal nerve fiber layer. Macular atrophy is noted in Family-B proband. There is increased retinal thickness in II-2 of Family-A. (**B**) Thickness of the GCL-IPL complex. The layer was consistently thicker in II-2 of Family-A.

a strong candidate gene for FFR. The *CRB1* variants were verified by Sanger sequencing and both variants segregated with the disease phenotype in the family; parents were carriers (I-1 carried p. Gly123Cys; I-2 carried p.Cys948Tyr). Both *SKOR1* variants, c.1897C > T/p.Arg633Trp and c.2260C > G/p.His754Asp (NM_001258024) were determined to be inherited paternally by Sanger sequencing, and thus excluded.

The novel exon 2 *CRB1* variant c.367G > T/p.Gly123Cys was not found in any of the control databases (1000 genomes, ExAC, NHLBI EVS, CG, dbSNP) and was well conserved in lower vertebrates up to Xenopus (Fig. 1D). The p.Gly123Cys change was predicted to be probably damaging by Polyphen with the highest score of 1.0, and SIFT categorized the change to be deleterious with the maximum score of 0. The variant c.2483G > A/p.Cys948Tyr in exon 9 of *CRB1* has earlier been associated with LCA, EORD and early onset RP.[7,8,23–28] It is the most frequent *CRB1* disease causing variant, and constitutes 152 of 1010 *CRB1* alleles registered in the Leiden Open Variation Database (in the public domain, http://databases.lovd.nl/shared/genes/CRB1). The cysteine at position 948 is well conserved in lower vertebrates such as Zebrafish (Fig. 1D).

The functional consequences of the two *CRB1* mutations can be rationalized by considering the folding of other epidermal growth factor–like (EGF-like) structures. Epidermal growth factor–like domains are often present in the extracellular domain of membrane-bound proteins or in proteins known to be secreted. The small (~40 amino acid) domains

Table 1. Whole-Exome Sequencing Filtering Steps in Family-A

Filtering Steps	Total Variants		
	Case II-1	Case II-2	Total Variants
Total variants	91,500	91,935	111,418
Coding variants	19,946	19,758	24,090
Nonsynonymous coding variants	9,432	9,390	11,518
Coding variants with allele frequency ≤ 0.01 (rare variants)	337	358	540
Shared rare variants (all heterozygous and homozygous)	NA	NA	175
Genes with ≥ 2 shared rare variants	NA	NA	9
Genes with 2 shared heterozygous variants	*9* *(Chr. 1) CRB1, IGFN1* *(Chr.5) PCDHGA8, PCDHGB7* *(Chr.15) SKOR1* *(Chr. 16) TBL3* *(Chr. 17) MYH13* *(Chr.19) ZNF780B, ZNF780A*		
Genes with shared homozygous variants	*None*		
Genes with known phenotypes	Autosomal recessive: *CRB1* Susceptibility: *PCDHGB7* (hypermethylation in non-Hodgkin's lymphoma); *SKOR1* Restless leg syndrome; *MYH13* (formal thought disorder)		

NA, Not applicable; Chr, chromosome.

Investigative Ophthalmology & Visual Science

Downloaded from iovs.arvojournals.org on 07/09/2021

Downloaded from iovs.arvojournals.org on 07/09/2021

Table 2. Pathogenicity Prediction of the Variants in the Nine Genes Shared Amongst the Sibship in Family-A

Gene	Chromosome/Genomic Position	RefSeq ID/Exon Number/Nucleotide Substitution/Amino Acid Substitution	Zygosity	Sift	Polyphen	Ma Score	CADD Phred	PhylopP Mam Avg	PhyloP Vert Avg	Cumulative Predicted Score (-/6)	ExAC Frequency
CRB1	chr1:197297848:G:T	NM_201253:exon2:c.G367T:p.G123C	Het	**0**	**1**	**4.325**	**15.58**	**2.854**	**5.749**	6	0
	chr1:197403836:G:A	NM_201253:exon9:c.G2843A:p.C948Y	Het	**0**	**0.996**	**2.915**	**15.23**	**2.479**	**8.753**	6	0.0002086
IGFN1	chr1:201181973:C:T	NM_001164586:exon12:c.C7952T:p.S2651F	Het	**0**	0.922	0	12.8	0.416	−0.806	1	0.01001
	chr1:201176303:G:A	NM_001164586:exon12:c.G2282A:p.R761Q	Het	0.16	NA	0	12.33	−2.011	−2.176	0	0.001433
PCDHGA8	chr5:140772679:C:T	NM_032088:exon1:c.C299T:p.P100L	Het	0.26	0.005	1.675	<0.001	0.213	−0.094	0	0.003169
	chr5:140773719:G:A	NM_032088:exon1:c.G1339A:p.D447N	Het	**0**	**1**	**4.35**	**17.76**	**2.366**	**9.781**	6	0.003260
PCDHGB7	chr5:140798377:A:G	NM_018927:exon1:c.A951G:p.I317M	Het	1	0.028	0.33	<0.001	0.069	−0.739	0	0.003142
	chr5:140797827:G:A	NM_018927:exon1:c.G401A:p.R134Q	Het	0.59	0.009	0.55	<0.001	−0.493	−5.487	0	0.003164
	chr5:140799449:T:A	NM_018927:exon1:c.T2023A:p.F675I	Het	0.14	0.002	−0.55	12.43	−0.434	−0.04	0	0.003121
SKOR1	chr15:68120354:C:T	NM_001258024:exon8:c.C1897T:p.R633W	Het	**0**	0.555	0.695	**17.94**	−0.679	0.583	2	0.004099
	chr15:68123191:C:G	NM_001258024:exon11:c.C2260G:p.H754D	Het	**0.02**	0.012	0	**16.51**	**2.564**	**5.015**	4	0.000008237
TBL3	chr16:2027115:C:T	NM_006453:exon15:c.C1501T:p.R501C	Het	**0.05**	**0.953**	1.89	**22.8**	**2.451**	**2.769**	5	0.0001829
	chr16:2028189:C:T	NM_006453:exon20:c.C2102T:p.A701V	Het	0.19	0.079	0.895	**15.71**	0.651	0.304	1	0.002177
MYH13	chr17:10231335:C:T	NM_003802:exon22:c.G2539A:p.A847T	Het	**0.05**	0.78	**2.16**	**20.8**	**2.235**	**4.821**	5	0.005350
	chr17:10267652:C:G	NM_003802:exon3:c.G196C:p.D66H	Het	0.07	0.921	1.955	11.97	**1.405**	0.917	1	0.000008842
ZNF780A	chr19:40582086:A:G	NM_001142577:exon6:c.T266C:p.V89A	Het	0.34	0.039	0.895	<0.001	−0.083	0.116	0	0.006495
	chr19:40580431:C:G	NM_001142577:exon6:c.G1921C:p.A641P	Het	0.15	0	−2.25	<0.001	−1.377	0.028	0	0.006171
ZNF780B	chr19:40540697:G:A	NM_001005851:exon5:c.C2069T:p.T690I	Het	1	0	1.08	<0.001	−0.261	−0.976	0	0.006187
	chr19:40540724:A:C	NM_001005851:exon5:c.T2042G:p.V681G	Het	0.21	0	−0.455	<0.001	−0.636	−3.127	0	0.006173

Het, heterozygous. Cut off values to predict pathogenicity for each of the six tools are as follows: Polyphen score $\geq$ 0.95; SIFT score $\leq$ 0.05, mutation assessor (Ma) score $\geq$ 2.0, CADD Phred score $\geq$ 15, Average PhyloP nucleotide conservation inferred from placental mammal-value $\geq$ 1.0 (PhyloP Mam Avg), and Average PhyloP nucleotide conservation inferred from vertebrate - value $\geq$ 1.0 (PhyloPVertAvg). Bolded cells represent SNV scores that met the pathogenicity cut-off value for a specific predictive tool. Cumulative predicted pathogenicity scores for each SNV were determined and shown in the far right column (-/6).

occur in tandem repeats, forming larger solenoid-like structures that bind calcium.[29,30] The disulphide bridges are key to the architecture of the EGF-like domains, and add rigidity to each repeat. The extracellular domain of CRB1 contains EGF-like domains, which have a typical structure containing six cysteine residues that form disulfide bridges with each other.[28] Loss of one of the cysteine residues at position 948 (p.Cys948Tyr) would disrupt formation of EGF-like domain #14 of CRB1 by eliminating a disulphide bond between Cys948 and Cys933 (disulphide denoted by # in Fig. 1C). The other mutation (p.Gly123Cys) occurs at the base of a turn within EGF-like repeat #3 of CRB1. Owing to steric flexibility, glycine is important to turn structures, and hence the mutant cysteine at position 123 would significantly affect the ability of the EGF-like region to properly form the solenoid-like structure (mutation denoted by * in Fig. 1C).[31] Because the oligomeric association of the EGF-like domains into the solenoid structures is important for protein function, any disruption of domain formation would affect the cellular role and activity of CRB1. Moreover, the cysteine residue at position 123 may form aberrant disulphide bonds with other cysteine residues, potentially leading to misfolding of the protein.

The WES results of the siblings were assessed for any rare coding sequence variants that could modify the disease phenotype. The CRB complex members (*CRB2*, *CRB3*, *MUPP1*, *MPP3*, *MPP4*, *MPP5*, and *PATJ*) and any other proteins that form the CRUMBS network (*CASK*, *DFNB31*, *DLG1*, *DLG4*, *EPB41L5*, *INADL*, *LIN7C*, *MPDZ*, and *SDCBP*)[32,33] were analyzed; no variants were seen shared among the siblings or found in either one of them in heterozygous or homozygous state. The WES results were also assessed for any rare, nonsynonymous, coding sequence variants in any of the known retinal dystrophy genes; no shared variants were observed, single heterozygous variants were seen in II-1 (*USH2A* and *CRX*) or in II-2 (*CC2D2A*; Supplementary Table S2).

Genetic Results: Family-B

In II-2, two presumed disease causing variants were observed in *CRB1* on WES analysis (c.498_506 del/p.Ile167_Gly169del and c.2290C > T/p.Arg764Cys). Both variants were confirmed by Sanger sequencing and segregated with the disease phenotype (Fig. 1B). The exon 2 variant, c.498_506 del/p.Ile167_Gly169del was not found in any of the control databases and has been earlier associated with early onset RP. [34] The exon 7 variant, c.2290C > T/ p.Arg764Cys has been previously associated with LCA, EORD and RP[4,7,8,23,28]; this variant is reported at extremely low frequency in ExAC (0.000099), never in a homozygous state. The residues p.Ile167 and p.Gly169 are conserved until vertebrates such as chicken and elephant respectively; the residues p.Asp168 and p.Arg764 are conserved in Rhesus (Fig. 1D). The deletion of the residues including p.Asp168 would affect the beta-turn of the EGF-like domain (^ in Fig. 1C). The p.Arg764Cys is located on the second laminin AG-like domain and is poorly conserved. Single heterozygous, rare, coding sequence nonsynonymous variants were noted in in *BBS7* and *CNGB3* (Supplementary Table S2). No rare nonsynonymous coding sequence variants were noted in any of the CRB complex members or in any protein that form part of the CRUMBS network.

Discussion

This is the first report implicating *CRB1* mutations to underlie FFR and confirms the autosomal recessive inheritance pattern of the disorder.[1] This report expands the phenotypic spectrum of *CRB1*-related disorders. The structural improvement (SD-OCT) of foveal schisis following topical Dorzolamide therapy was not associated with any significant improvement of visual function. The disease is of early onset and demonstrates stable vision parameters into early adulthood[1,2] but may show some deterioration and macular atrophy in later stages.

Schitic/cystoid change at the macula is the diagnostic retinal anomaly in FFR, and found in Family-A, and the right eye of the Family-B proband in the current study. In 2014, Tsang et al.[9] used WES to establish *CRB1* as the genetic basis of an unusual maculopathy in a sib-ship (1 male, 1 female; p.Arg1331Cys/p.Pro1381Leu) who had mottled granularly-speckled maculopathy along with paramacular annular RPE atrophy extending nasal to the disc. The unusual maculopathy phenotype spared the peripheral retina and one of the individuals also had cystoid macular changes.[9] Recently, Wolfson et al.[10] reported female twins with mild foveal RPE mottling, cystoid macular edema and moderately reduced amplitudes of cone full-field ERGs to harbor homozygous p.Pro836Thr mutations in *CRB1*. *CRB1*-related RP, EORD, and complex disease (nanopthalmos-RP-optic disc drusen) have also been variably associated with cystic/schitic changes at the macula.[8,11,26] Taken together, cystoid/schitic macular changes appear to be a feature of *CRB1*-related retinopathies with the exception of LCA.

Full-field rod and cone ERGs were normal in all affected cases in the current study excluding any generalized rod and cone dysfunction or loss of function, consistent with FFR.[1] In the maculopathy phenotype described by Tsang et al.,[9] rod and cone ERG amplitudes were normal; however, cone ERG implicit times were delayed which suggested mild generalized cone dysfunction. In the *CRB1*-related maculopathy phenotype reported by Wolfson et al.,[10] the ERGs showed a moderate generalized cone dystrophy phenotype. These findings suggest that *CRB1*-related maculopathies could show a range of electrophysiological phenotypes.

In flies, the Crumbs protein is required for appropriate photoreceptor morphogenesis, assembly of adherens junction, and maintenance of apico-basal photoreceptor cell polarity.[6,35,36] Mouse mutant models of *Crb1* show disruptions in the outer limiting membrane and focal loss of adherens junction; subsequently, focal loss of adhesion between photoreceptors and Müller cells ensue, which leads to displacement of photoreceptors that form pseudorosettes and progressive retinal disorganization.[37–40] A recent study reports a spontaneous rat mutant of *Crb1* to demonstrate extensive cystoid changes in the inner and outer retinal layers in addition to progressive retinal degeneration and retinal telangiectasia.[41] Increased retinal thickness with loss of lamination is a relatively constant feature of *CRB1*-related human LCA, EORD, and RP.[8,38] However, in the current study, retinal lamination appeared normal; retinal lamination was also reported normal in the sibship in the unusual maculopathy phenotype.[9] The increased central retinal thickness in the sibship (Family-A) in the current study is predominantly a consequence of the persistent schitic changes at the level of inner and outer nuclear layers and GCL. The SD-OCT segmentation analysis showed GCL-IPL complex thickness to be normal (II-1; Family-A), borderline increased (II-2; Family-B), or markedly increased (case II-2; Family-A).

Both p.Cys948Tyr and p.Arg764Cys variants found in this report have been previously associated with LCA, EORD, and RP in both homozygous and compound heterozygous states.[4,7,8,23–28] The p.Ile167_Gly169del variant has been associated with early onset RP in homozygous and compound heterozygous forms. The p.Pro836Thr variant recently associated with *CRB1*-maculopathy (Wolfson et al.[10]) in homozygous state, has previously been associated with RP (homozygous)[26]

Investigative Ophthalmology & Visual Science

Downloaded from iovs.arvojournals.org on 07/09/2021

and EORD (compound heterozygous).[8] The p.Pro1381Leu variant associated with unusual *CRB1*-maculopathy in compound heterozygous state (Tsang et al.)[9] has previously been associated with LCA (compound heterozygous).[8] This suggests genetic and/or environmental factors modifying the expression of the *CRB1* phenotype. In the present study, no nonsynonymous rare coding sequence variants were found in any other CRB proteins or any protein in the CRUMBS network in any of the affected individuals.

Disease-causing mutations of residues present in the EGF-like domains of *CRB1* have been described previously. In particular, of the 43 mutations in *CRB1* that cause RP (RP12), 17 are present in EGF-like domains, 22 are present in laminin G-like domains and four are outside of these structural regions. Similarly, for LCA (LCA8), 17 mutations occur in the EGF-like domains, 17 in the laminin G-like domains, and 2 are outside of these regions (in the public domain, www.uniprot.org). The severity of each of these mutations would depend highly on the characterization of the mutation (which amino acid substitution occurs, deletion, or premature stop codon) and the role of that particular EGF-like or laminin G-like region in protein–protein interactions or in the formation of multiprotein tandem repeats. How these mutations alter the protein structure and protein interactions likely is what defines the severity and character of the clinical phenotype.

Macular schitic/cystoid changes are also found in a wide variety inherited retinal disorders that include RP, X-linked retinoschisis, enhanced S-cone syndrome, choroideremia, gyrate atrophy, autosomal recessive bestrophinopathy, autosomal recessive maculopathy, and dominant cystoid macular dystrophy.[1,9,10,42–49] In the majority of the disorders, carbonic anhydrase inhibitors (CAI) have been shown to have modest effect in the treatment of the cystoid changes.[50] The current study reports for the first time that CAI reduces schitic changes in FFR. It is noted that other *CRB1* maculopathies also show improvement with CAI.[9,10]

Recently, a new entity termed stellate nonhereditary idiopathic foveo-macular retinoschisis (SNIFR) has been proposed to accommodate sporadic cases of unilateral or bilateral macular schisis; 94% (16/17) of the cases were females.[51] It is possible that some of these cases represent isolated foveal retinoschisis and may harbor mutations in *CRB1*.

To conclude, FFR is an autosomal recessive condition due to mutations in *CRB1*. This is the first report of a male subject with isolated/familial foveal retinoschisis. Mutations in *CRB1* result in a range of autosomal recessive retinal dystrophies that vary in severity, age of onset, and extent of retinal involvement; FFR represents the mildest end of the spectrum of *CRB1*-related diseases known to date. *CRB1*-related maculopathy phenotypes may or may not show generalized retinal involvement; the ERG helps in its ascertainment. Schitic or cystoid changes may be a frequent finding in *CRB1*-related maculopathy phenotypes. It is intriguing that *CRB1*, a gene cardinal in retinal development causes FFR without generalized retinal dysfunction, the reason for which remains to be elucidated.

Acknowledgments

The authors wish to thank the The Centre for Applied Genomics, Toronto, Canada for the contribution of the high throughput sequencing platform of. The authors also thank Cynthia Vanden Hoven, Leslie MacKeen, and Peter Breitschmid for their contribution of ophthalmic imaging and assistance in figure design. Finally, the authors thank the families for their enthusiastic participation in the study.

Supported by the Mira Godard Research fund (EH; Toronto, Ontario, Canada), and University of Toronto McLaughlin Center Accelerator Grant (EH; Toronto, Ontario, Canada), and Clinical Research Priority program at University of Zurich (JH; Zurich, Switzerland).

Disclosure: **A. Vincent**, None; **J. Ng**, None; **C. Gerth-Kahlert**, None; **E. Tavares**, None; **J.T. Maynes**, None; **T. Wright**, None; **A. Tiwari**, None; **A. Tumber**, None; **S. Li**, None; **J.V.M. Hanson**, R; **A. Bahr**, None; **H. MacDonald**, None; **L. Bähr**, None; **C. Westall**, None; **W. Berger**, None; **F.P.M. Cremers**, None; **A.I. den Hollander**, None; **E. Héon**, None

References

1. Lewis RA, Lee GB, Martonyi CL, Barnett JM, Falls HF. Familial foveal retinoschisis. *Arch Ophthalmol*. 1977;95:1190–1196.
2. Kabanarou SA, Holder GE, Bird AC, et al. Isolated foveal retinoschisis as a cause of visual loss in young females. *Br J Ophthalmology*. 2003;87:801–803.
3. Chen FK, McAllister IL, Chelva ES. Thirteen-year follow up of isolated foveal retinoschisis in a 24-year-old woman. *Clin Exp Ophthalmol*. 2006;34:600–605.
4. den Hollander AI, ten Brink JB, de Kok YJ, et al. Mutations in a human homologue of Drosophila crumbs cause retinitis pigmentosa (RP12). *Nat Genet*. 1999;23:217–221.
5. den Hollander AI, Johnson K, de Kok YJ, et al. CRB1 has a cytoplasmic domain that is functionally conserved between human and Drosophila. *Human Mol Genet*. 2001;10:2767–2773.
6. Tepass U. Crumbs, a component of the apical membrane, is required for zonula adherens formation in primary epithelia of Drosophila. *Dev Biol*. 1996;177:217–225.
7. den Hollander AI, Heckenlively JR, van den Born LI, et al. Leber congenital amaurosis and retinitis pigmentosa with Coats-like exudative vasculopathy are associated with mutations in the crumbs homologue 1 (CRB1) gene. *Am J Human Genet*. 2001;69:198–203.
8. Henderson RH, Mackay DS, Li Z, et al. Phenotypic variability in patients with retinal dystrophies due to mutations in CRB1. *Br J Ophthalmol*. 2011;95:811–817.
9. Tsang SH, Burke T, Oll M, et al. Whole exome sequencing identifies CRB1 defect in an unusual maculopathy phenotype. *Ophthalmology*. 2014;121:1773–1782.
10. Wolfson Y, Applegate CD, Strauss RW, Han IC, Scholl HP. CRB1-related maculopathy with cystoid macular edema. *JAMA Ophthalmol*. 2015;133:1357–1360.
11. Paun CC, Pijl BJ, Siemiatkowska AM, et al. A novel crumbs homolog 1 mutation in a family with retinitis pigmentosa, nanophthalmos, and optic disc drusen. *Mol Vis*. 2012;18:2447–2453.
12. Marmor MF, Fulton AB, Holder GE, Miyake Y, Brigell M, Bach M. ISCEV standard for full-field clinical electroretinography (2008 update). *Doc Ophthalmol*. 2009;118:69–77.
13. McCulloch DL, Marmor MF, Brigell MG, et al. ISCEV Standard for full-field clinical electroretinography (2015 update). *Doc Ophthalmol*. 2015;130:1–12.
14. Abramoff MD, Garvin MK, Sonka M. Retinal Imaging and Image Analysis. *IEEE Trans Med Imaging*. 2010;3:169–208.
15. Li K, Wu X, Chen DZ, Sonka M. Optimal surface segmentation in volumetric images–a graph-theoretic approach. *IEEE Trans Pattern Anal Mach Intel*. 2006;28:119–134.
16. Chen X, Niemeijer M, Zhang L, Lee K, Abramoff MD, Sonka M. Three-dimensional segmentation of fluid-associated abnormalities in retinal OCT: probability constrained graph-search-graph-cut. *IEEE Trans Med Imaging*. 2012;31:1521–1531.
17. Grading diabetic retinopathy from stereoscopic color fundus photographs–an extension of the modified Airlie House

Investigative Ophthalmology & Visual Science

Downloaded from iovs.arvojournals.org on 07/09/2021

classification. ETDRS report number 10. Early Treatment Diabetic Retinopathy Study Research Group. *Ophthalmology*. 1991;98(suppl 5):786–806.

18. Vincent A, Forster N, Maynes JT, et al. OTX2 mutations cause autosomal dominant pattern dystrophy of the retinal pigment epithelium. *J Med Genet*. 2014;51:797–805.
19. Adzhubei IA, Schmidt S, Peshkin L, et al. A method and server for predicting damaging missense mutations. *Nat Methods*. 2010;7:248–249.
20. Kumar P, Henikoff S, Ng PC. Predicting the effects of coding non-synonymous variants on protein function using the SIFT algorithm. *Nat Protoc*. 2009;4:1073–1081.
21. Reva B, Antipin Y, Sander C. Predicting the functional impact of protein mutations: application to cancer genomics. *Nucleic Acids Res*. 2011;39:e118.
22. Kircher M, Witten DM, Jain P, O'Roak BJ, Cooper GM, Shendure J. A general framework for estimating the relative pathogenicity of human genetic variants. *Nat Genet*. 2014;46:310–315.
23. Lotery AJ, Jacobson SG, Fishman GA, et al. Mutations in the CRB1 gene cause Leber congenital amaurosis. *Arch Ophthalmol*. 2001;119:415–420.
24. Tosi J, Tsui I, Lima LH, Wang NK, Tsang SH. Case report: autofluorescence imaging and phenotypic variance in a sibling pair with early-onset retinal dystrophy due to defective CRB1 function. *Curr Eye Res*. 2009;34:395–400.
25. Riveiro-Alvarez R, Vallespin E, Wilke R, et al. Molecular analysis of ABCA4 and CRB1 genes in a Spanish family segregating both Stargardt disease and autosomal recessive retinitis pigmentosa. *Mol Vision*. 2008;14:262–267.
26. Bujakowska K, Audo I, Mohand-Said S, et al. CRB1 mutations in inherited retinal dystrophies. *Human Mut*. 2012;33:306–315.
27. Booij JC, Florijn RJ, ten Brink JB, et al. Identification of mutations in the AIPL1, CRB1, GUCY2D, RPE65, and RPGRIP1 genes in patients with juvenile retinitis pigmentosa. *J Med Genet*. 2005;42:e67.
28. den Hollander AI, Davis J, van der Velde-Visser SD, et al. CRB1 mutation spectrum in inherited retinal dystrophies. *Human Mutat*. 2004;24:355–369.
29. Chaturvedi P, Singh AP, Batra SK. Structure, evolution, and biology of the MUC4 mucin. *FASEB J*. 2008;22:966–981.
30. Jonckheere N, Skrypek N, Frenois F, Van Seuningen I. Membrane-bound mucin modular domains: from structure to function. *Biochimie*. 2013;95:1077–1086.
31. Malkov SN, Zivkovic MV, Beljanski MV, Hall MB, Zaric SD. A reexamination of the propensities of amino acids towards a particular secondary structure: classification of amino acids based on their chemical structure. *J Mol Model*. 2008;14:769–775.
32. Alves CH, Pellissier LP, Wijnholds J. The CRB1 and adherens junction complex proteins in retinal development and maintenance. *Progr Retin Eye Res*. 2014;40:35–52.
33. Gosens I, den Hollander AI, Cremers FP, Roepman R. Composition and function of the Crumbs protein complex in the mammalian retina. *Exp Eye Res*. 2008;86:713–726.
34. Corton M, Tatu SD, Avila-Fernandez A, et al. High frequency of CRB1 mutations as cause of early-onset retinal dystrophies in the Spanish population. *Orphanet J Rare Dis*. 2013;8:20.
35. Pellikka M, Tanentzapf G, Pinto M, et al. Crumbs, the Drosophila homologue of human CRB1/RP12, is essential for photoreceptor morphogenesis. *Nature*. 2002;416:143–149.
36. Tepass U. Adherens junctions: new insight into assembly, modulation and function. *Bioessays*. 2002;24:690–695.
37. Mehalow AK, Kameya S, Smith RS, et al. CRB1 is essential for external limiting membrane integrity and photoreceptor morphogenesis in the mammalian retina. *Human Mol Genet*. 2003;12:2179–2189.
38. Aleman TS, Cideciyan AV, Aguirre GK, et al. Human CRB1-associated retinal degeneration: comparison with the rd8 Crb1-mutant mouse model. *Invest Ophthalmol Vis Sci*. 2011;52:6898–6910.
39. van de Pavert SA, Kantardzhieva A, Malysheva A, et al. Crumbs homologue 1 is required for maintenance of photoreceptor cell polarization and adhesion during light exposure. *J Cell Sci*. 2004;117(Pt 18):4169–4177.
40. van de Pavert SA, Sanz AS, Aartsen WM, et al. Crb1 is a determinant of retinal apical Müller glia cell features. *Glia*. 2007;55:1486–1497.
41. Zhao M, Andrieu-Soler C, Kowalczuk L, et al. A new CRB1 rat mutation links Müller glial cells to retinal telangiectasia. *J Neurosci*. 2015;35:6093–6106.
42. Genead MA, Fishman GA. Cystic macular oedema on spectral-domain optical coherence tomography in choroideremia patients without cystic changes on fundus examination. *Eye (Lond)*. 2011;25:84–90.
43. Haider NB, Jacobson SG, Cideciyan AV, et al. Mutation of a nuclear receptor gene, NR2E3, causes enhanced S cone syndrome, a disorder of retinal cell fate. *Nat Genet*. 2000;24:127–131.
44. Vincent A, Robson AG, Neveu MM, et al. A phenotype-genotype correlation study of X-linked retinoschisis. *Ophthalmology*. 2013;120:1454–1464.
45. Fishman GA, Fishman M, Maggiano J. Macular lesions associated with retinitis pigmentosa. *Arch Ophthalmol*. 1977;95:798–803.
46. Feldman RB, Mayo SS, Robertson DM, Jones JD, Rostvold JA. Epiretinal membranes and cystoid macular edema in gyrate atrophy of the choroid and retina. *Retina*. 1989;9:139–142.
47. Saksens NT, van Huet RA, van Lith-Verhoeven JJ, den Hollander AI, Hoyng CB, Boon CJ. Dominant cystoid macular dystrophy. *Ophthalmology*. 2015;122:180–191.
48. Boon CJ, van den Born LI, Visser L, et al. Autosomal recessive bestrophinopathy: differential diagnosis and treatment options. *Ophthalmology*. 2013;120:809–820.
49. Fung AT, Yzer S, Goldberg N, et al. New best1 mutations in autosomal recessive bestrophinopathy. *Retina*. 2015;35:773–782.
50. Salvatore S, Fishman GA, Genead MA. Treatment of cystic macular lesions in hereditary retinal dystrophies. *Surv Ophthalmol*. 2013;58:560–584.
51. Ober MD, Freund KB, Shah M, et al. Stellate nonhereditary idiopathic foveomacular retinoschisis. *Ophthalmology*. 2014;121:1406–1413.
52. Kershaw NJ, Church NL, Griffin MD, Luo CS, Adams TE, Burgess AW. Notch ligand delta-like1: x-ray crystal structure and binding affinity. *Biochem J*. 2015;468:159–166.

Investigative Ophthalmology & Visual Science

Downloaded from iovs.arvojournals.org on 07/09/2021